https://dx.doi.org/10.1016/j.envpol.2017.01.013

$PM_{2.5}$ in the Yangtze River Delta, China: chemical compositions, seasonal variations, and regional pollution events

Lili Ming[a], Ling Jin[a], Jun Li[b], Pingqing Fu[c], Wenyi Yang[c], Di Liu[b], Gan Zhang[b], Zifa Wang[c], and Xiangdong Li[a, *]

[a]*Department of Civil and Environmental Engineering, The Hong Kong Polytechnic University, Hung Hom, Kowloon, Hong Kong*

[b]*State Key Laboratory of Organic Geochemistry, Guangzhou Institute of Geochemistry, Chinese Academy of Sciences, Guangzhou, 510640, China*

[c]*LAPC, Institute of Atmospheric Physics, Chinese Academy of Sciences, Beijing 100029, China*

*Corresponding author

E-mail: cexdli@polyu.edu.hk (X.D. Li); Tel.: +852-27666041; Fax: +852-23346389.

Abstract

Fine particle ($PM_{2.5}$) samples were collected simultaneously at three urban sites (Shanghai, Nanjing, and Hangzhou) and one rural site near Ningbo in the Yangtze River Delta (YRD) region, China, on a weekly basis from September 2013 to August 2014. In addition, high-frequency daily sampling was conducted in Shanghai and Nanjing for one month during each season. Severe regional $PM_{2.5}$ pollution episodes were frequently observed in the YRD, with annual mean concentrations of 94.6 ± 55.9, 97.8 ± 40.5, 134 ± 54.3, and 94.0 ± 57.6 μg m^{-3} in Shanghai, Nanjing, Hangzhou, and Ningbo, respectively. The concentrations of $PM_{2.5}$ and ambient trace metals at the four sites showed clear seasonal trends, with higher concentrations in the winter and lower concentrations in the summer. In Shanghai, similar seasonal patterns were found for organic carbon (OC), elemental carbon (EC), and water-soluble inorganic ions (K^+, NH_4^+, Cl^-, NO_3^-, and SO_4^{2-}). Backward air trajectory and potential source contribution function (PSCF) analyses implied that areas of central and northern China contributed significantly to the concentration and chemical compositions of $PM_{2.5}$ in Shanghai during winter. Three heavy pollution events in Shanghai were observed during autumn

and winter. The modelling results of the Nested Air Quality Prediction Modeling System (NAQPMS) showed the sources and transport of $PM_{2.5}$ in the YRD during the three pollution processes. The contribution of secondary species (SOC, NH_4^+, NO_3^-, and SO_4^{2-}) in pollution event (PE) periods was much higher than in BPE (before pollution event) and APE (after pollution event) periods, suggesting the importance of secondary aerosol formation during the three pollution events. Furthermore, the bioavailability of Cu, and Zn in the wintertime $PM_{2.5}$ samples from Shanghai was much higher during the pollution days than during the non-pollution days.

Keywords: Secondary aerosol, Primary organic carbon, Potential source contribution function; Nested air quality prediction modeling system; Bioavailability;

Capsule: Secondary aerosol formation is important and the bioavailability of trace metals is much higher during the pollution events.

1. Introduction

Elevated fine particulate matter ($PM_{2.5}$) in the atmosphere has become a top environmental concern, due to their adverse effects on human health (Wessels et al., 2010) and climate change (Huang et al., 2012). When breathed, $PM_{2.5}$ can reach the deepest regions of our lungs and may cause a wide range of health problems (Lanki et al., 2006; Wessels et al., 2010). An epidemiological association between human exposure to $PM_{2.5}$ and increases in the incidence of mortality and morbidity due to lung cancer and cardiovascular diseases has been demonstrated in a number of studies (Corbett et al., 2007; Viana et al., 2008). The adverse effects of fine particles have also been attributed to the toxicological effects of chemical compounds associated with fine particles (Gerlofs-Nijland et al., 2009; Uzu et al., 2011), such as organic carbon (OC) and elemental carbon (EC), and water-soluble inorganic ions and metal elements (such as Fe, Cu, Pb, Zn, Ni, and V). The inhalation of $PM_{2.5}$ can therefore have a long-term and serious impact on human health.

In recent years, the occurrence of $PM_{2.5}$ pollution has become increasingly frequent on a large scale in China (Fu et al., 2008; Hu et al., 2014), indicating that

$PM_{2.5}$ pollution is no longer confined in individual cities but expanding over a large regional scale. In some previous studies, the characteristics, chemical compositions, sources, and formation mechanism of $PM_{2.5}$ in some megacities of China, such as Guangzhou, Shanghai, Nanjing, and Beijing have been investigated (Wang et al., 2006a; Yang et al., 2005; Yao et al., 2002). However, very few investigations of $PM_{2.5}$ have been conducted on a regional scale in China, such as those carried out in the Beijing-Tianjin-Hebei area (Zhao et al., 2013) and the Pearl River Delta (PRD) region (Hagler et al., 2006). The Yangtze River Delta (YRD) region is the most economically developed and rapidly urbanizing city cluster in eastern China. Due to the high levels of energy consumption and large emissions of atmospheric pollutants, and to the influence of the East Asian monsoon on long-range transport in the YRD region (Wang et al., 2008), air pollution was severe in the YRD in recent years (Feng et al., 2009; Shen et al., 2014). The characteristics of $PM_{2.5}$ have been individually studied at a city scale (Cao et al., 2009; Chen et al., 2008), but in very few studies has synchronous sampling been conducted in different cities of the YRD region over an annual cycle. It is imperative to generate a high-quality database of the concentration and chemical compositions of $PM_{2.5}$ on a regional scale. Moreover, regional pollution events such that affect the entire YRD region have become more frequent in recent years (Fu et al., 2008; Wang et al., 2015). Previous studies focused on the formation mechanism of pollution events by monitoring air pollutants (Fu et al., 2010; Fu et al., 2008). Recently, a 3-D model, the Nested Air Quality Prediction Modeling System (NAQPMS), has been applied to understand the sources and transport of air pollutants (Li et al., 2008; Li et al., 2014; Wang et al., 2006c). This encourages us to integrate monitoring data and modeling results to better understand the formation and evolution of $PM_{2.5}$ pollution events.

In this study, $PM_{2.5}$ samples were simultaneously collected in four cities of the YRD region over a one-year period to analyze the aerosol chemical compositions including metal elements, OC and EC, and water-soluble inorganic ions. A 3-D chemical transport model, NAQPMS, was applied to simulate the formation and

evolution of $PM_{2.5}$ during pollution events. The objectives of this study were to characterize the seasonal variations and potential sources of $PM_{2.5}$, identify the characteristics of chemical components and the formation and evolution of pollution events, and evaluate the bioavailability of airborne trace metals on pollution days and non-pollution days.

2. Experiment and Methods

2.1 Field Sampling

Three urban sites in large cities – Shanghai (SH), Nanjing (NJ), and Hangzhou (HZ), and one rural site in Ningbo (NB) were selected for field sampling in the YRD region (Fig. 1). Details of the sampling sites are described in Table S1. The $PM_{2.5}$ samples were collected on 8 × 10 inch quartz microfiber filters (PALL, USA) using a high-volume sampler equipped with a 2.5 μm inlet at a flow rate of 1 m^3/min. Before sampling, all the filters were pre-baked for 6 h at 500 °C to remove any contamination caused by carbonaceous materials. The filters were weighed twice, once before and once after sampling, using a balance (Sartorius Analytic, Gottingen, Germany) with a sensitivity of ± 0.1 mg. After sampling, the loaded filters were covered with aluminum foil and stored in polyethylene bags at -20 °C before being analyzed. Simultaneously, weekly sampling (*i.e.*, one 24-h sample per week) was conducted at each of the four sampling sites from September 2013 to August 2014. In addition, more intensive daily $PM_{2.5}$ sampling (*i.e.*, one 24-h sample per day) was conducted simultaneously in Shanghai and Nanjing in autumn (from 16 October 2013 to 14 November 2013), winter (from 21 December 2013 to 20 January 2014), spring (from 21 March 2014 to 20 April 2014), and summer (from 23 June 2014 to 23 July 2014). We selected these two high energy consumption cites with typical geographical contrast (coastal for Shanghai and inland for Nanjing) to conduct the intensive daily sampling, enabling us to compare the field observation results between the cities and investigate the regional transport of $PM_{2.5}$ in the YRD. At each site, two field blank filters (one for 24 h and the other for the whole sampling period) were placed into the high-volume sampler in a non-

working state to check the background contamination from the field. Meanwhile, laboratory blank filters were stored at a clean desiccators at 20-30 °C for checking background contamination from the lab. The concentrations of all the chemicals in blank filters and field blank filters were less than 1% of the average analyte concentrations for all the chemicals. A total of 143, 119, 45, and 44 samples were collected at the SH, NJ, HZ, and NB sites, respectively.

2.2 Chemical Analysis and Quality Control

Total concentrations of major and trace elements were analysed for each filtered $PM_{2.5}$ sample collected from all the four cities. Concentrations of OC, EC, water-soluble ions (NO_3^-, Cl^-, SO_4^{2-}, K^+ and NH_4^+) and bioavailable metal fractions were analyzed only for the samples from Shanghai.

To analyze the total concentrations of major and trace elements, one-eighth of the filter was cut and put into acid-cleaned Pyrex test tubes (18 mm ×18 mm) (Wong et al., 2003). About 12 mL of 70% high-purity nitric acid (HNO_3) and 3 mL of 65% perchloric acid ($HClO_4$) were added to ensure that the filters were completely submerged. The mixed solutions were gently shaken using a vortex, and then heated progressively to 190 °C in an aluminum heating block to complete dryness. Twelve mL of 5% (v/v) high-purity HNO_3 were added, and then heated at 70 °C for 1 h. After cooling, the solutions were poured into 15 mL plastic tubes for storage at 4 °C until analysis. All glass and plastic tubes were acid cleaned and rinsed with deionized water before use. Quality control was carried out by analyzing reagent blanks, replicates, and standard reference materials (NIST SRM 1648a, urban particulate matter), representing 10, 10, and 10% of the total number of samples, respectively. Trace metals concentrations were determined using an Inductively Coupled Plasma - Optical Emission Spectrometer (ICP-OES, Agilent 720) after calibration using 5% high-purity HNO_3. Regent blanks (5% high-purity HNO_3) and quality control standards were measured at every 10 samples to detect contamination and drift. The concentrations of trace metals in regent blanks were < 1% of the average analyte concentrations for all of the targeted metals,

and the recovery rates of the metal elements in the standard reference material (NIST SRM 1648a) ranged from 96-110% (with the exception of 54% for Al without HF in the digestion).

The analysis of OC, EC, and water-soluble inorganic ions followed previously described procedures as provided in the SI. Based on the EC-tracer method (Castro et al., 1999) (details in the SI), the concentrations of primary organic carbon (POC) and secondary organic carbon (SOC) were also estimated. Simulated lung fluids – Gamble's solution were used to extract the soluble fraction of trace metals in the 21 selected $PM_{2.5}$ samples collected in SH from 5 December 2013 to 17 January 2014. Gamble's solution was freshly prepared according to the procedure described by Colombo et al. (2008). Details of the extraction procedures and analytical determination are provided in the SI.

2.3 Back Trajectory and Potential Source Contribution Function

Air mass backward trajectories were calculated at 6-hour intervals for sampling days at an elevation of 500 m AGL (above ground level) using the Hybrid-Single Particle Integrated Trajectories (HYSPLIT 4.9) developed by the National Oceanic and Atmospheric Administration (NOAA) Air Resource Laboratory (http://www.arl.noaa.gov/HYSPLIT.php). All of the backward trajectories were classified into several types through cluster analysis based on the non-hierarchical clustering algorithm (Dorling et al., 1992). The Potential Sources Contribution Function (PSCF) model is similar to the framework described by Ashbaugh et al. (1985). The movement of an air parcel during sampling periods is described using segment endpoints of coordinates in terms of latitude and longitude (Zhang et al., 2014). All of the hourly endpoints in the back trajectories generated by the HYSPLIT 4.9 were classified into 1º latitude by 1º longitude grid cells to avoid uncertainties in the calculations. The PSCF value for the *ij*-th cell was defined as

$$PSCF_{(i,j)} = m_{(i,j)}/n_{(i,j)} \quad (1)$$

where $m_{(i,j)}$ is the number of endpoints corresponding to measured pollutant concentrations higher than a given criterion value, which is set to the mean concentration of each pollutant during the sampling period. $n_{(i,j)}$ is the total number of endpoints falling in the grid cell. All values were plotted using mapping software (ArcMap 10.2). Only a given cell that included a total of more than 10 hourly points was plotted. Because the synoptic atmospheric conditions at the four cities were quite similar, back trajectory and PSCF analyses were conducted only in Shanghai in this study.

2.4 Model Description and Setup

The Nested Air Quality Prediction Modeling System (NAQPMS) was used in this study to simulate the evolution of $PM_{2.5}$ over eastern China during the three pollution events. NAQPMS is a multi-scale 3-D Euler chemical transport model that was developed by the Institute of Atmospheric Physics (IAP), Chinese Academy of Sciences (Wang et al., 2006c). The Weather Research and Forecasting Model (WRF version 3.5) was used as a meteorological driver for NAQPMS. The nested chemical transport module includes advection and diffusion processes (Byun and Dennis, 1995; Walcek and Aleksic, 1998), and the parameterization of the dry and wet deposition of pollutants (Wesely, 1989). The Carbon-Bond mechanism Z (CBM-Z) (Zaveri and Peters, 1999), which contains 133 reactions for 53 species, was used to represent the gas phase chemistry in NAQPMS. The composition and phase state of an ammonia-sulfate-nitrate-chloride-sodium-water inorganic aerosol were calculated using the model ISORROPIA 1.7 (Nenes et al., 1998); and the secondary organic aerosols (SOA) were predicted based on a two-product yield scheme (Odum et al., 1997). A detailed description of the calculation and prediction can be found in previous work (Li et al., 2008). The modeling domains consisted of a 27-km horizontal grid covering East Asia and a 9-km nested grid over eastern China (Fig. S1). The vertical structure of the model consisted of 20 layers from the surface to 20 km above the surface, with the lowest ten layers below 2 km. The lateral and upper boundary conditions were taken from a global

chemical transport model (MOZART-V2.4) with a 2.8º resolution. The anthropogenic emission inventory was obtained from the bottom-up Regional Emission inventory in Asia (REAS2.1) data with a 0.25º×0.25º resolution (Kurokawa et al., 2013). Biomass burning emissions were developed by Cao et al. (2005) and resampled to a daily time step based on MODIS fire hot spots in 2010 with a 1.0º×1.0º resolution. Monthly biogenic emissions were generated by MEGAN v2.0, a biogenic emission model with a 0.5º×0.5º resolution provided by NCAR (the National Center for Atmospheric Research) (http://accent.aero.jussieu.fr/database_table_inventories.php).

3. Results and Discussion

3.1 Concentrations of $PM_{2.5}$ and Chemical Components

The annual means of $PM_{2.5}$ at the SH, NJ, HZ, and NB sites were 94.6 ± 55.9, 97.8 ± 40.5, 134 ± 54.3, and 94.0 ± 57.6 μg m^{-3}, respectively, which were 9 to 13 times the standard set by the World Health Organization (WHO) of 10 μg m^{-3}, and 2 to 3 times the Chinese National Ambient Air Quality Standards' (NAAQS) Grade II of 35 μg m^{-3}. It is interesting to note that the rural mountainous site of Ningbo displayed similarly high pollution levels to other urban sites during the polluted seasons, indicating that regional pollution events overwrote the local background with no known emission sources surrounding the area. The annual concentrations of $PM_{2.5}$ in the YRD region were lower than those in northern China, such as Baoding (118 μg m^{-3}) and Xingtai (109 μg m^{-3}), but higher than those in the PRD region, such as Guangzhou (42.4 μg m^{-3}), Zhuhai (33.8 μg m^{-3}), and Shenzhen (32.0 μg m^{-3}) (Zhang and Cao, 2015), and those in other countries, such as USA (Abu-Allaban et al., 2007), Korea (Choi et al., 2012), and Greece (Samara et al., 2014). $PM_{2.5}$ concentrations for the spontaneous samples taken in the four cities (Fig. 2a) and for the samples collected during the high-frequency sampling period in SH and NJ (Fig. 2b) showed similar fluctuations, respectively. The results indicate a similar regional pollution pattern for $PM_{2.5}$ in the YRD to that found in northern China (Luo et al., 2014) and the North China Plain (Hu et al., 2014). The concentrations and temporal variations of $PM_{2.5}$ were similar for all the studied cities within each region. The regional $PM_{2.5}$ pollution pattern also suggests that a significant

fraction of the $PM_{2.5}$ could be secondary particles, which have regional sources and a wide distribution pattern (Fu et al., 2010; Fu et al., 2008).

The annual average concentrations of airborne trace metals at the four sites are listed in Table 1. The major abundant metal elements are crustal elements (e.g., Al, Ca, Fe, and Mg), but they only account for 3.34-4.76% of the mass concentrations of $PM_{2.5}$. The concentrations of trace metals are in the order of Zn > Pb > Cu > Cr > V > Ni. At present, there are no regulated standards for metal loadings in $PM_{2.5}$ in China. However, the level of Ni in the winter season in SH exceeded the WHO threshold value of Ni (20 ng m^{-3}) in PM_{10} (WHO, 2000). Compared with past monitoring data in the YRD region, such as Shanghai (annual mean, 2009-2010) (Chen et al., 2008), Nanjing (average value from April to September 2010) (Hu et al., 2012), and Hangzhou (annual mean, 2006) (Bao et al., 2010), the concentrations of Zn in SH, and Cu and Zn in NJ and HZ showed a decreasing trend, probably due to the more stringent regulations on the emissions of trace metals from various sources, such as steel industry, other heavy industries, and vehicle emissions in the YRD region (CCICED, 2014). However, the levels of ambient trace metals in the YRD region were still higher than those in some other countries, such as Southern California (Na and Cocker III, 2009) and Turkey (Kendall et al., 2011).

In Shanghai, the high-frequency samples were analyzed for OC and EC, and the weekly samples for water-soluble ions in $PM_{2.5}$. The average concentrations of OC and EC and water-soluble ions in $PM_{2.5}$ in SH are presented in Table 2. The annual mean concentrations of OC and EC in SH were 9.89 ± 8.89 and 1.63 ± 1.53 μg m^{-3}, respectively, which contributed 9.85 ± 3.40% and 1.62 ± 0.77% of the $PM_{2.5}$ mass, respectively. The results were consistent with those in a previous study conducted at the campus of Fudan University in Shanghai by Feng et al. (2006). In comparison with other urban cities in China, the OC and EC concentrations were lower than the values obtained in Beijing (Zhao et al., 2013) and Guangzhou (Duan et al., 2007). The secondary inorganic ions, including NO_3^-, SO_4^{2-}, and NH_4^+, are the dominant ionic species in SH. The annual mean concentrations of NO_3^-, SO_4^{2-}, and NH_4^+ were 18.0 ±

19.1, 14.5 ± 9.61, and 8.13 ± 6.99 μg m^{-3}, respectively, which constituted 12.7 ± 7.7%, 12.9 ± 6.20%, and 6.39 ± 3.54% of the $PM_{2.5}$ mass, respectively.

3.2 Seasonal variations in the Concentration and Chemical Compositions of $PM_{2.5}$

Clear seasonal patterns of $PM_{2.5}$ and airborne trace metals were observed in the YRD region (Table 1). At the urban sites of SH, NJ, and HZ, the average concentrations of $PM_{2.5}$ and trace metals were higher in the winter and lower in the summer, which is similar to other air pollutants in this region (Cao et al., 2009; Wang et al., 2006b). However, high levels of crustal elements were also observed in NJ in the spring, probably due to the influence of dust storms from western and northern China under the northwestern monsoon in the spring (Hsu et al., 2009; Lee et al., 2010; Wang et al., 2007). The concentrations of $PM_{2.5}$ and airborne trace metals were lowest in the summer at the rural site of NB, but no significant differences were found among the autumn, winter, and spring seasons. As shown in Table 2, the OC, EC, and water-soluble ions in Shanghai exhibited seasonal patterns similar to those of the $PM_{2.5}$ and airborne trace metals. The seasonal patterns of atmospheric pollutants in the YRD are related to local, regional and remote sources. Meteorological conditions, particularly the seasonal monsoons that carry pollutants originating from regional and remote sources, strongly influence the relative contribution of each source to the pollutant levels detected locally (Liu et al., 2013). The results of the backward air mass trajectory analysis and cluster analysis in Shanghai showed that the air masses were seasonally dependent (Fig. S2). Maps of the potential sources of $PM_{2.5}$ in Shanghai during the four seasons are displayed in Fig. 3. The PSCF result identified areas of central China including the provinces of Henan, Hubei, and Anhui, and northern China as the major potential source regions of $PM_{2.5}$ during the winter (Fig. 3b). Li et al. (2014) also noted that central China, the North China Plain, and northeast China contributed 16.0%, 9.4%, and 6.5% of PM_{10} mass concentrations in eastern China in winter, respectively. The intensive emissions of air pollutants from coal combustion for heating in northern China (Zhao et al., 2013) and the high concentrations of $PM_{2.5}$ pollution in central

China during winter (Cao et al., 2012) could have contributed to the increase in $PM_{2.5}$ and other air pollutants in SH. In summer, regional and remote sources became dwarfed by local sources as the influence of the air masses from the north weakened. Given the clean marine air masses from the East China Sea (Fig. 3d), remarkably lower $PM_{2.5}$ concentrations were thus recorded in summer than in winter.

3.3 Mechanisms for the Formation of Pollution Events

3.3.1 Identification of Three Pollution Events

During the high-frequency sampling periods, three heavy pollution events were simultaneously observed in Shanghai and Nanjing (Fig. 2b). Pollution events were defined by the daily average visibility (<10 Km) and relative humidity (<80%) (details in the SI). The first pollution event occurred from 5 to 11 November 2013, which can be divided into the period before the pollution event (BPE1 period: 5-6 November), the period of the pollution event (PE1 period: 7-8 November), and the period after the pollution event (APE1 period: 9-11 November). During PE1, the average $PM_{2.5}$ concentrations were 188 and 143 μg m^{-3} in Shanghai and Nanjing, respectively. Fig. 4a shows the one-day backward trajectories of the air masses that arrived in SH during PE1 from the inland areas of Jiangsu and Anhui provinces, in contrast to those in the BPE1 and APE1 periods when clean air masses came from the eastern coastal region. The air masses from the inland areas of Jiangsu and Anhui provinces may have contributed to PE1. A severe and long-lasting pollution event (PE2) occurred in the YRD region from 5 to 12 December 2013. There was no apparent period before and after the pollution event. In Shanghai, $PM_{2.5}$ concentrations peaked on 6 December at an extremely high level of 395 μg m^{-3} and then decreased but remained above 100 μg m^{-3}. As shown by the backward trajectory analysis (Fig. 4b), short-range air masses from the YRD occurred from 5 to 8 December, while long-range air masses occurred from 10 to 12 December. During PE2, the high $PM_{2.5}$ concentrations that occurred during 5-8 December may be attributed to the accumulation of $PM_{2.5}$ under low wind speeds in the YRD region, and the $PM_{2.5}$ pollution was alleviated from 10 to 12

December due to a fast-moving cold front hitting the YRD region (Wang et al., 2015). The process of the third pollution event is divided into the period before the pollution event (BPE3 period: 22-24 December 2013), the period of the pollution event (PE3 period: 25 December 2013 to 4 January 2014) and the period after the pollution event (APE3 period: 5-7 January 2014). The average concentrations of $PM_{2.5}$ during PE3 were 182 and 150 μg m^{-3} in SH and NJ, respectively. As shown in Fig. 4c, air masses arrived in SH from the northwest that originated from northern China and travelled over central China during PE3, different from that during the BPE3 and APE3 periods when clean air masses originated from the ocean. Thus, the influence of air masses from northern China and central China may have contributed to the high $PM_{2.5}$ pollution in PE3.

3.3.2 Modeling Results

The simulated daily average of surface $PM_{2.5}$ concentrations and wind fields displayed the sources and transport of $PM_{2.5}$ during the three pollution events in the YRD. Prior to PE1, on 5 November, the prevailing easterly winds coming from the ocean with high wind speeds favored low $PM_{2.5}$ concentrations of less than 75 μg m^{-3} in the YRD (Fig. 5a). On 6 November, the dominant westerly winds clearly showed that high concentrations of $PM_{2.5}$ over Anhui, Henan, and Shandong provinces were transported from the west to the east in the YRD (Fig. 5b). After that, a high $PM_{2.5}$ event occurred in the YRD with low wind speeds on 7 November, with the concentration of $PM_{2.5}$ being higher in the eastern part of the YRD (Fig. 5c). The field observation also confirmed that the concentration of $PM_{2.5}$ was higher in Shanghai during PE1 than in the other three sites. From 8 November, the strong sea winds carrying clean air masses from the southeast dispersed $PM_{2.5}$ pollution northwestward, resulting in the alleviation of PE1 in the YRD (Fig. 5d). During the early stage of PE2 (Fig. 5e and 5f), stable wind field and high concentrations of $PM_{2.5}$ of more than 300 μg m^{-3} (shaded in dark blue) were observed in the YRD. On 9 December, strong northerly winds prevailed over eastern China, driving air masses rapidly over the region of the YRD with high concentrations of $PM_{2.5}$ (Fig. 5g). Under northerly wind

conditions, $PM_{2.5}$ pollution over the YRD region weakened on 11 December (Fig. 5h). At the beginning of PE3, on 26 December, a high $PM_{2.5}$ region was observed in the YRD, but strong northerly winds prevailed over eastern China, bringing clean air from northern China (Fig. 6a). From 31 December, the wind field changed, forcing the high $PM_{2.5}$ air over central China from the west to the YRD (Fig. 6b). On 2 January 2014, a high $PM_{2.5}$ zone over the YRD was transported from the southeast to the northwest under the prevailing southeasterly winds (Fig. 6c). As shown in Fig. 6d, strong northeasterly winds from the East China Sea dominated the YRD region on 4 January 2014, driving the high concentrations of $PM_{2.5}$ from the northern part of the YRD to the East China Sea. After that, the high levels of $PM_{2.5}$ in the YRD dropped. The modeling results showed the same variation trend of $PM_{2.5}$ as the field observations during the processes of the three pollution events.

3.3.3 Chemical Compositions

As shown in Fig. 7a, the concentrations of all of the measured chemical components in PE1 were much higher than in the BPE1 and APE1 periods. The concentrations of SOC, NO_3^-, SO_4^{2-}, and NH_4^+ during PE1 were 3-6 times higher than those in the BPE1 and APE1 periods, indicating the large contribution of secondary fractions to the PE1. The contribution of SOC to total organic carbon was up to 80% during PE1 (Fig. 7d), which also suggests the importance of the formation of secondary organic aerosol in driving $PM_{2.5}$ pollution during the pollution events (Huang et al., 2014). NO_3^-, SO_4^{2-}, and NH_4^+, were the dominant components of $PM_{2.5}$, accounting for 29.3%, 18.0%, and 11.2% of the $PM_{2.5}$ mass in PE1, respectively. NO_3^- and SO_4^{2-} are formed by gas-particle conversion processes from nitrogen oxides (NO_x) and sulfur dioxide (SO_2) in the atmosphere into the particulate phase, respectively. In urban environments, the major sources of NO_x emissions are the combustion of fossil fuels and traffic emissions, while emissions of SO_2 come mainly from industrial activities (Seinfeld and Pandis, 2012) . The ratio of NO_3^- to SO_4^{2-} has been used as an indicator of the relative contributions to aerosol particles from mobile vs. stationary sources of S and N (Cao et al., 2009; Wang et al., 2006b). The average value of NO_3^-/SO_4^{2-} (1.64)

during PE1 was higher than that in BPE1 (0.58) and APE1 (1.18), revealing that more NO_x had been released mainly from vehicular emissions. During APE1, when the southeast sea winds prevailed, SO_4^{2-} instead of NO_3^- became the dominant secondary ions. Marine aerosols contain little NO_3^-, which is mainly formed through the anthropogenic sources. However, SO_4^{2-} can be formed via the photooxidation of dimethylsulphide in the marine atmosphere (Calhoun et al., 1991). The high SO_4^{2-}/NO_3^- ratios during APE1 may reflect the influence of marine aerosol. The concentration of K^+ in $PM_{2.5}$ during PE1 was 4 times higher than that in the BPE1 and APE1 periods, different from other crustal metals, such as Al, Fe, Ca, and Mg, which increased only two-fold compared to the non-pollution days. The greater increase in K^+ suggested the contribution of enhanced biomass burning activities to PE1 (Urban et al., 2012). The high ratio of OC/EC in PE1 (with an average value of 10.3) also support the presence of emissions from the burning of biomass. These results suggested that vehicular emissions and the burning of biomass are the key contributors of PE1 in Shanghai.

During PE2, the concentrations of chemical components were extremely higher than those on the normal days, especially on 6 December (Fig. 7b). The secondary inorganic ions were the major chemical components, accounting for 52.3% of the $PM_{2.5}$ mass. Similar to PE1, a high ratio of NO_3^-/SO_4^{2-} (with an average value of 1.54) in PE2 indicated serious pollution from vehicle exhaust in Shanghai. Interestingly, in PE2 the concentrations of chemical components displayed a different tendency to vary. After the peak values on 6 December, the concentrations of all the measured chemicals were declined from 7 to 9 December. During 10-12 December, the concentrations of SOC, secondary inorganic ions and trace metals showed a steady decline, while the concentrations of POC, EC and crustal metals showed an increasing trend. As shown in Fig. 7e, the relative abundance of SOC was as steadily high as ~80% during 5-9 December, and the relative abundance of POC increased gradually from ~20% to ~50% after 9 December. The stable meteorological conditions during 5-9 December favored the accumulation of local or regional air pollutants and the formation of secondary aerosols, and the cold front during 10-12 December introduced more remote inputs of

POC and crustal metals.

Elevated concentrations for all chemical components were observed during PE3, compared with the BPE3 and APE3 periods (Fig. 7c). Compared to PE1 and PE2, the concentrations of SOC and secondary inorganic ions in PE3 were much lower, but the concentrations of the measured primary components, including POC, EC, and crustal metals, were higher during PE3. As indicated in Fig. 7f, an increasing trend in the relative abundance of POC and a declining trend in the relative abundance of SOC were measured during PE3 in comparison with BPE3 and APE3 periods. Fig. 8 shows the relative abundance of chemical components for $PM_{2.5}$ in Shanghai during the three events. The dominance of SOC and secondary inorganic ions in all the three pollution events suggests the importance of secondary aerosol formation during the three pollution events. By comparison, the dominances of secondary components were more remarkable in PE1 and PE2, while the abundances of the measured primary components were highest in PE3. Based on the above backward trajectory and modeling analysis, the occurrence of PE1 and PE2 was related to the accumulation of air contaminants in the YRD under stable meteorological conditions, while the formation of PE3 was more influenced by the regional transport of air pollutants under different wind directions.

3.4 Bioavailability of Airborne Trace Metals in $PM_{2.5}$

The soluble fraction of trace metals in PM is most likely to be bioaccessible and correlated with their potential toxicities (Valavanidis et al., 2005). In this study, the bioavailability of trace metals in $PM_{2.5}$ in the wintertime $PM_{2.5}$ samples from Shanghai was measured by their soluble fractions extracted by simulated lung fluids. The mean soluble concentrations and fractions of trace metals on pollution days and non-pollution days are listed in Table 3. Compared with the non-pollution days, the soluble concentrations of Cu ($p<0.05$) and Zn ($p<0.01$) were found to be significantly higher on pollution days, suggesting the elevated mobility and toxic potential of these two metals during the pollution days. Non-statistically significant differences in soluble concentrations of Cr, Pb, V and Ni were found between the pollution days and the non-

pollution days. The mobilized mean fractions in $PM_{2.5}$ varied among trace metals, with large soluble fractions for V (69.9~83.7%) and Cu (27.8~41.4%), and small soluble fractions for Ni (22.9~26.3%), Pb (17.2~19.2%), Cr (10.8~15.5%), and Zn (4.45~17.1%). The mean solubility of trace metals was comparable to that reported in $PM_{2.5}$ from Frankfurt, Germany using Gamble's solution as the extractant for 24 h (Wiseman and Zereini, 2014), but slightly higher than that of $PM_{2.5}$ samples from Beijing, China using water for the extraction test (Schleicher et al., 2011). The use of simulated lung fluid does provide more real bioavailability of airborne metals in comparison to using water as a leaching agent, as it is more likely to reflect the real conditions of a human body (Mukhtar and Limbeck, 2013). High soluble fractions of Cu, and Zn were also found on pollution days, probably due to differences in emission sources and chemical components between pollution and non-pollution days. The toxic effect posed by Cu during the pollution days may be worthy of further examination because of its high soluble fraction and high concentration in $PM_{2.5}$. Although the soluble fractions of Pb and Zn were small, their high soluble concentrations during the pollution days remain a potential toxic risk in comparison with the non-pollution days.

4. Conclusions

The annual average concentrations of $PM_{2.5}$ were 94.0 to 134 μg m^{-3} at the four sites in the YRD region, with more than 60% of the measurements exceeding the NAAQS of 75 μg m^{-3}. The concentrations of ambient trace metals in the YRD region were still high. The annual mean concentrations of OC and EC in Shanghai were 9.89 ± 8.89 and 1.63 ± 1.53 μg m^{-3}, respectively. NO_3^-, SO_4^{2-}, and NH_4^+ were found to be the dominant ionic species in Shanghai, constituting 31.9 ± 14.9% of the $PM_{2.5}$ mass. Distinct seasonal patterns were found in the concentrations of $PM_{2.5}$ and associated chemical compositions, with higher concentrations during the winter than during the summer. Back trajectory and PSCF analyses showed that areas of central and northern China, where enhanced burning of coal and biomass for domestic heating occurs in winter, contributed significantly to the levels of $PM_{2.5}$ and air pollutants measured in the YRD during the season. Three pollution events in Shanghai were identified by field

observations and model results (NAQPMS). The chemical components of $PM_{2.5}$, meteorological conditions, and the source region and transport of air contaminants during the pollution processes were shown. Secondary species (SOC and secondary inorganic ions) were the major chemical components of $PM_{2.5}$ in the three pollution events. In addition, the bioavailability of Cu and Zn in the wintertime $PM_{2.5}$ samples from Shanghai was higher on the pollution days than in the non-pollution days.

Acknowledgments

This work was supported by the Research Grants Council of Hong Kong SAR Government (PolyU 152095/14E), The Hong Kong Polytechnic University (1-ZE16) and National Natural Science Foundation of China (91543205). The authors would like to thank the students from the research group of Prof. Zhigang Guo (Department of Environmental Science and Engineering, Fudan University), Prof. Daohui Lin (College of Environmental and Resource Sciences, Zhejiang University), and Dr. Long Cang (Institute of Soil Science, Chinese Academy of Sciences) for their assistance in the field sampling program.

References

Abu-Allaban, M., Gillies, J.A., Gertler, A.W., Clayton, R., Proffitt, D., 2007. Motor vehicle contributions to ambient PM_{10} and $PM_{2.5}$ at selected urban areas in the USA. Environ. Monit. Assess. 132, 155-163.

Ashbaugh, L.L., Malm, W.C., Sadeh, W.Z., 1985. A residence time probability analysis of sulfur concentrations at Grand Canyon National Park. Atmos. Environ. 19, 1263-1270.

Bao, Z., Fen, Y.C., Jiao, L., Hong, S.M., Liu, W.G., 2010. Charaterization and source apportionment of $PM_{2.5}$ and PM_{10} in Hangzhou. Environ. Monit. in China 26, 44-48 (in Chinese).

Byun, D.W., Dennis, R., 1995. Design artifacts in Eulerian air quality models: evaluation of the effects of layer thickness and vertical profile correction on surface ozone concentrations. Atmos. Environ. 29, 105-126.

Calhoun, J.A., Bates, T.S., Charlson, R.J., 1991. Sulfur isotope measurements of submicrometer sulfate aerosol particles over the Pacific Ocean. Geophys. Res. Lett. 18, 1877–1880.

Cao, G.L., Zhang, X.Y., Wang, D., Zheng, F.C., 2005. Inventory of atmospheric pollutants discharged from biomass burning in China continent. China Environ. Sci. 25, 389-393 (in Chinese).

Cao, J.J., Shen, Z.X., Chow, J.C., Qi, G.W., Watson, J.G., 2009. Seasonal variations and sources of mass and chemical composition for PM_{10} aerosol in Hangzhou, China. Particuology 7, 161-168.

Cao, J.J., Shen, Z.X., Chow, J.C., Watson, J.G., Lee, S.C., Tie, X.X., Ho, K.F., Wang, G.H., Han, Y.M., 2012. Winter and summer $PM_{2.5}$ chemical compositions in fourteen Chinese cities. J. Air Waste

493 Manage. Assoc. 62, 1214-1226.
494 Castro, L.M., Pio, C.A., Harrison, R.M., Smith, D.J.T., 1999. Carbonaceous aerosol in urban and rural
495 European atmospheres: estimation of secondary organic carbon concentrations. Atmos. Environ.
496 33, 2771-2781.
497 CCICED, 2014. Performance evaluation on the action plan of air pollution prevention and control and
498 regional coordination mechanism, Online available:
499 http://www.cciced.net/encciced/policyresearch/report/201504/P020150413497618655390.pdf.
500 Chen, J.M., Tan, M.G., Li, Y.L., Zheng, J., Zhang, Y.M., Shan, Z.C., Zhang, G.L., Li, Y., 2008.
501 Characteristics of trace elements and lead isotope ratios in $PM_{2.5}$ from four sites in Shanghai. J.
502 Hazard. Mater. 156, 36-43.
503 Choi, J.K., Heo, J.B., Ban, S.J., Yi, S.M., Zoh, K.D., 2012. Chemical characteristics of $PM_{2.5}$ aerosol in
504 Incheon, Korea. Atmos. Environ. 60, 583-592.
505 Colombo, C., Monhemius, A.J., Plant, J.A., 2008. Platinum, palladium and rhodium release from vehicle
506 exhaust catalysts and road dust exposed to simulated lung fluids. Ecotoxicol. Environ. Saf. 71,
507 722-730.
508 Corbett, J.J., Winebrake, J.J., Green, E.H., Kasibhatla, P., Eyring, V., Lauer, A., 2007. Mortality from
509 ship emissions: a global assessment. Environ. Sci. Technol. 41, 8512-8518.
510 Dorling, S.R., Davies, T.D., Pierce, C.E., 1992. Cluster analysis: a technique for estimating the synoptic
511 meteorological controls on air and precipitation chemistry—method and applications. Atmospheric
512 Environment. Part A. General Topics 26, 2575-2581.
513 Duan, J.C., Tan, J.H., Cheng, D.X., Bi, X.H., Deng, W.J., Sheng, G.Y., Fu, J.M., Wong, M.H., 2007.
514 Sources and characteristics of carbonaceous aerosol in two largest cities in Pearl River Delta
515 Region, China. Atmos. Environ. 41, 2895-2903.
516 Feng, J.L., Chan, C.K., Fang, M., Hu, M., He, L.Y., Tang, X.Y., 2006. Characteristics of organic matter
517 in $PM_{2.5}$ in Shanghai. Chemosphere 64, 1393-1400.
518 Feng, Y.L., Chen, Y.J., Guo, H., Zhi, G.R., Xiong, S.C., Li, J., Sheng, G.Y., Fu, J.M., 2009.
519 Characteristics of organic and elemental carbon in $PM_{2.5}$ samples in Shanghai, China. Atmos. Res.
520 92, 434-442.
521 Fu, Q.Y., Zhuang, G.S., Li, J., Huang, K., Wang, Q.Z., Zhang, R., Fu, J., Lu, T., Chen, M., Wang, Q.,
522 2010. Source, long-range transport, and characteristics of a heavy dust pollution event in Shanghai.
523 J. Geophys. Res. 115.
524 Fu, Q.Y., Zhuang, G.S., Wang, J., Xu, C., Huang, K., Li, J., Hou, B., Lu, T., Streets, D.G., 2008.
525 Mechanism of formation of the heaviest pollution episode ever recorded in the Yangtze River Delta,
526 China. Atmos. Environ. 42, 2023-2036.
527 Gerlofs-Nijland, M.E., Rummelhard, M., Boere, A.J.F., Leseman, D.L., Duffin, R., Schins, R.P., Borm,
528 P.J., Sillanpää, M., Salonen, R.O., Cassee, F.R., 2009. Particle induced toxicity in relation to
529 transition metal and polycyclic aromatic hydrocarbon contents. Environ. Sci. Technol. 43, 4729-
530 4736.
531 Hagler, G.S.W., Bergin, M.H., Salmon, L.G., Yu, J.Z., Wan, E.C.H., Zheng, M., Zeng, L.M., Kiang, C.S.,
532 Zhang, Y.H., Lau, A.K.H., 2006. Source areas and chemical composition of fine particulate matter
533 in the Pearl River Delta region of China. Atmos. Environ. 40, 3802-3815.
534 Hsu, S.C., Liu, S.C., Arimoto, R., Liu, T.H., Huang, Y.T., Tsai, F., Lin, F.J., Kao, S.J., 2009. Dust
535 deposition to the East China Sea and its biogeochemical implications. J. Geophys. Res. 114.
536 Hu, J.L., Wang, Y.G., Ying, Q., Zhang, H.L., 2014. Spatial and temporal variability of $PM_{2.5}$ and PM_{10}

over the North China Plain and the Yangtze River Delta, China. Atmos. Environ. 95, 598-609.
Hu, X., Zhang, Y., Ding, Z.H., Wang, T.J., Lian, H.Z., Sun, Y.Y., Wu, J.C., 2012. Bioaccessibility and health risk of arsenic and heavy metals (Cd, Co, Cr, Cu, Ni, Pb, Zn and Mn) in TSP and $PM_{2.5}$ in Nanjing, China. Atmos. Environ. 57, 146-152.
Huang, K., Zhuang, G., Lin, Y., Fu, J.S., Wang, Q., Liu, T., Zhang, R., Jiang, Y., Deng, C., Fu, Q., Hsu, N.C., Cao, B., 2012. Typical types and formation mechanisms of haze in an Eastern Asia megacity, Shanghai. Atmos. Chem. Phys. 12, 105-124.
Huang, R.J., Zhang, Y.l., Bozzetti, C., Ho, K.F., Cao, J.J., Han, Y.M., Daellenbach, K.R., Slowik, J.G., Platt, S.M., Canonaco, F., 2014. High secondary aerosol contribution to particulate pollution during haze events in China. Nature 514, 218-222.
Kendall, M., Pala, K., Ucakli, S., Gucer, S., 2011. Airborne particulate matter ($PM_{2.5}$ and PM_{10}) and associated metals in urban Turkey. Air Qual. Atmos. Health 4, 235-242.
Kurokawa, J., Ohara, T., Morikawa, T., Hanayama, S., Janssens-Maenhout, G., Fukui, T., Kawashima, K., Akimoto, H., 2013. Emissions of air pollutants and greenhouse gases over Asian regions during 2000–2008: Regional Emission inventory in ASia (REAS) version 2. Atmos. Chem. Phys. 13, 11019-11058.
Lanki, T., de Hartog, J.J., Heinrich, J., Hoek, G., Janssen, N.A., Peters, A., Stölzel, M., Timonen, K.L., Vallius, M., Vanninen, E., 2006. Can we identify sources of fine particles responsible for exercise-induced ischemia on days with elevated air pollution? The ULTRA study. Environ. Health Perspect. 114, 655-660.
Lee, Y., Yang, X., Wenig, M., 2010. Transport of dusts from East Asian and non-East Asian sources to Hong Kong during dust storm related events 1996–2007. Atmos. Environ. 44, 3728-3738.
Li, J., Wang, Z., Akimoto, H., Yamaji, K., Takigawa, M., Pochanart, P., Liu, Y., Tanimoto, H., Kanaya, Y., 2008. Near-ground ozone source attributions and outflow in central eastern China during MTX2006. Atmos. Chem. Phys. 8, 7335-7351.
Li, J., Yang, W.Y., Wang, Z.F., Chen, H.S., Hu, B., Li, J.J., Sun, Y.L., Huang, Y., 2014. A modeling study of source–receptor relationships in atmospheric particulate matter over Northeast Asia. Atmos. Environ. 91, 40-51.
Liu, D., Li, J., Zhang, Y.L., Xu, Y., Liu, X., Ding, P., Shen, C.D., Chen, Y.J., Tian, C.G., Zhang, G., 2013. The use of levoglucosan and radiocarbon for source apportionment of $PM_{2.5}$ carbonaceous aerosols at a background site in East China. Environ. Sci. Technol. 47, 10454-10461.
Luo, X.S., Ip, C.C.M., Li, W., Tao, S., Li, X.D., 2014. Spatial–temporal variations, sources, and transport of airborne inhalable metals (PM_{10}) in urban and rural areas of northern China. Atmos. Chem. Phys. Discuss 14, 13133-13165.
Mukhtar, A., Limbeck, A., 2013. Recent developments in assessment of bio-accessible trace metal fractions in airborne particulate matter: a review. Anal. Chim. Acta 774, 11-25.
Na, K., Cocker III, D.R., 2009. Characterization and source identification of trace elements in $PM_{2.5}$ from Mira Loma, Southern California. Atmos. Res. 93, 793-800.
Nenes, A., Pandis, S.N., Pilinis, C., 1998. ISORROPIA: A new thermodynamic equilibrium model for multiphase multicomponent inorganic aerosols. Aquat. Geochem. 4, 123-152.
Odum, J.R., Jungkamp, T., Griffin, R., Flagan, R.C., Seinfeld, J.H., 1997. The atmospheric aerosol-forming potential of whole gasoline vapor. Science 276, 96-99.
Samara, C., Voutsa, D., Kouras, A., Eleftheriadis, K., Maggos, T., Saraga, D., Petrakakis, M., 2014. Organic and elemental carbon associated to PM_{10} and $PM_{2.5}$ at urban sites of northern Greece.

Environ. Sci. Pollut. Res. 21, 1769-1785.
Schleicher, N.J., Norra, S., Chai, F.H., Chen, Y.Z., Wang, S.L., Cen, K., Yu, Y., Stüben, D., 2011. Temporal variability of trace metal mobility of urban particulate matter from Beijing–A contribution to health impact assessments of aerosols. Atmos. Environ. 45, 7248-7265.
Seinfeld, J.H., Pandis, S.N., 2012. Atmospheric chemistry and physics: from air pollution to climate change. John Wiley & Sons.
Shen, G.F., Yuan, S.Y., Xie, Y.N., Xia, S.J., Li, L., Yao, Y.K., Qiao, Y.Z., Zhang, J., Zhao, Q.Y., Ding, A.J., 2014. Ambient levels and temporal variations of $PM_{2.5}$ and PM_{10} at a residential site in the mega-city, Nanjing, in the western Yangtze River Delta, China. J. Environ. Sci. Heal. A. 49, 171-178.
Urban, R.C., Lima-Souza, M., Caetano-Silva, L., Queiroz, M.E.C., Nogueira, R.F.P., Allen, A.G., Cardoso, A.A., Held, G., Campos, M.L.A.M., 2012. Use of levoglucosan, potassium, and water-soluble organic carbon to characterize the origins of biomass-burning aerosols. Atmos. Environ. 61, 562-569.
Uzu, G., Sauvain, J.J., Baeza-Squiban, A., Riediker, M., Sánchez Sandoval Hohl, M., Val, S., Tack, K., Denys, S., Pradère, P., Dumat, C., 2011. In vitro assessment of the pulmonary toxicity and gastric availability of lead-rich particles from a lead recycling plant. Environ. Sci. Technol. 45, 7888-7895.
Valavanidis, A., Vlahoyianni, T., Fiotakis, K., 2005. Comparative study of the formation of oxidative damage marker 8-hydroxy-2'-deoxyguanosine (8-OHdG) adduct from the nucleoside 2'-deoxyguanosine by transition metals and suspensions of particulate matter in relation to metal content and redox reactivity. Free Radic. Res 39, 1071-1081.
Viana, M., Querol, X., Alastuey, A., Ballester, F., Llop, S., Esplugues, A., Fernández-Patier, R., García dos Santos, S., Herce, M.D., 2008. Characterising exposure to PM aerosols for an epidemiological study. Atmos. Environ. 42, 1552-1568.
Walcek, C.J., Aleksic, N.M., 1998. A simple but accurate mass conservative, peak-preserving, mixing ratio bounded advection algorithm with FORTRAN code. Atmos. Environ. 32, 3863-3880.
Wang, M.Y., Cao, C.X., Li, G.S., Singh, R.P., 2015. Analysis of a severe prolonged regional haze episode in the Yangtze River Delta, China. Atmos. Environ. 102, 112-121.
Wang, X.H., Bi, X.H., Sheng, G.Y., Fu, J.M., 2006a. Chemical composition and sources of PM_{10} and $PM_{2.5}$ aerosols in Guangzhou, China. Environ. Monit. Assess. 119, 425-439.
Wang, Y., Chai, F.H., Liu, H.F., Wang, Y.H., 2008. Analysis on the charateristics of horizontal transport of the atmospheric pollutant over the Yangtze Delta. Res. Environ. Sci. 21, 22-29 (in Chinese).
Wang, Y., Zhuang, G.S., Tang, A.H., Zhang, W.J., Sun, Y.L., Wang, Z.F., An, Z.S., 2007. The evolution of chemical components of aerosols at five monitoring sites of China during dust storms. Atmos. Environ. 41, 1091-1106.
Wang, Y., Zhuang, G.S., Zhang, X.Y., Huang, K., Xu, C., Tang, A.H., Chen, J.M., An, Z.S., 2006b. The ion chemistry, seasonal cycle, and sources of $PM_{2.5}$ and TSP aerosol in Shanghai. Atmos. Environ. 40, 2935-2952.
Wang, Z.F., Li, J., Wang, X.Q., Pochanart, P., Akimoto, H., 2006c. Modeling of regional high ozone episode observed at two mountain sites (Mt. Tai and Huang) in East China. J. Atmos. Chem. 55, 253-272.
Wesely, M., 1989. Parameterization of surface resistances to gaseous dry deposition in regional-scale numerical models. Atmos. Environ. 23, 1293-1304.
Wessels, A., Birmili, W., Albrecht, C., Hellack, B., Jermann, E., Wick, G., Harrison, R.M., Schins, R.P.,

625 2010. Oxidant generation and toxicity of size-fractionated ambient particles in human lung
626 epithelial cells. Environ. Sci. Technol. 44, 3539-3545.
627 WHO, 2000. Air quality guidelines for Europe, 2nd edn. World Health Organization, Regional Office
628 for Europe, Copenhagen.
629 Wiseman, C.L., Zereini, F., 2014. Characterizing metal (loid) solubility in airborne PM_{10}, $PM_{2.5}$ and PM_1
630 in Frankfurt, Germany using simulated lung fluids. Atmos. Environ. 89, 282-289.
631 Wong, C.S.C., Li, X.D., Zhang, G., Qi, S.H., Peng, X.Z., 2003. Atmospheric deposition of heavy metals
632 in the Pearl River Delta, China. Atmos. Environ. 37, 767-776.
633 Yang, H., Yu, J.Z., Ho, S.S.H., Xu, J.H., Wu, W.S., Wan, C.H., Wang, X.D., Wang, X.R., Wang, L.S.,
634 2005. The chemical composition of inorganic and carbonaceous materials in $PM_{2.5}$ in Nanjing,
635 China. Atmos. Environ. 39, 3735-3749.
636 Yao, X.H., Chan, C.K., Fang, M., Cadle, S., Chan, T., Mulawa, P., He, K., Ye, B.M., 2002. The water-
637 soluble ionic composition of $PM_{2.5}$ in Shanghai and Beijing, China. Atmos. Environ. 36, 4223-
638 4234.
639 Zaveri, R.A., Peters, L.K., 1999. A new lumped structure photochemical mechanism for large-scale
640 applications. J. Geophys. Res. 104, 30387-30415.
641 Zhang, F., Cheng, H.R., Wang, Z.W., Lv, X.P., Zhu, Z.M., Zhang, G., Wang, X.M., 2014. Fine particles
642 ($PM_{2.5}$) at a CAWNET background site in Central China: Chemical compositions, seasonal
643 variations and regional pollution events. Atmos. Environ. 86, 193-202.
644 Zhang, Y.L., Cao, F., 2015. Fine particulate matter ($PM_{2.5}$) in China at a city level. Scientific reports
645 5:14884.
646 Zhao, P.S., Dong, F., He, D., Zhao, X.J., Zhang, X.L., Zhang, W.Z., Yao, Q., Liu, H.Y., 2013.
647 Characteristics of concentrations and chemical compositions for $PM_{2.5}$ in the region of Beijing,
648 Tianjin, and Hebei, China. Atmos. Chem. Phys. 13, 4631-4644.
649

650

651 Table 1. The annual and seasonal average concentrations of $PM_{2.5}$ and airborne trace metals at the four sites of the YRD region.

Locations		μg m^{-3}				ng m^{-3}						
		$PM_{2.5}$	Al	Ca	Fe	Mg	Cr	Cu	Pb	Zn	V	Ni
Shanghai	Annual (n=143)	94.6	0.922	1.93	1.34	298	16.9	24.2	69.7	215	16.5	14.9
	Autumn (n=33)	75.2	0.746	1.62	1.18	274	18.5	20.0	65.4	202	13.3	12.4
	Winter (n=40)	138	1.20	2.72	1.85	415	25.5	45.7	137	359	23.1	23.6
	Spring (n=41)	95.7	1.08	1.94	1.37	327	12.3	17.2	43.2	161	17.5	14.2
	Summer (n=29)	55.5	0.515	1.17	0.752	124	9.80	9.06	19.2	104	9.87	6.71
Nanjing	Annual (n=119)	97.8	0.705	1.52	0.942	209	13.2	24.7	90.9	247	9.88	9.30
	Autumn (n=29)	98.3	0.763	1.52	1.16	220	16.1	32.5	111	337	14.2	10.1
	Winter (n=31)	130	0.716	1.67	1.05	249	24.4	36.8	149	349	15.9	15.8
	Spring (n=30)	97.6	0.933	2.22	1.18	278	7.90	20.4	64.9	193	6.80	7.60
	Summer (n=29)	63.5	0.401	0.651	0.362	42.2	3.80	8.5	36.1	106	1.70	3.20
Hangzhou	Annual (n=45)	134	1.37	3.02	1.72	446	17.9	38.5	122	495	15.3	10.4
	Autumn (n=10)	108	1.25	3.10	1.73	470	24.5	39.3	130	604	29.0	13.4
	Winter (n=13)	182	2.05	4.56	2.48	749	31.8	75.4	228	821	19.5	18.8
	Spring (n=11)	138	1.48	3.03	1.73	419	9.40	19.6	63.6	313	8.60	5.60
	Summer (n=11)	101	0.707	1.44	0.970	151	6.00	18.6	62.3	254	5.50	3.60
Ningbo	Annual (n=44)	96.2	1.17	1.19	1.16	216	14.6	16.2	56.3	190	7.36	8.25
	Autumn (n=10)	102	1.58	1.82	1.57	259	12.8	24.1	78.5	281	7.72	10.1
	Winter (n=13)	114	1.28	1.60	1.71	280	21.3	22.2	81.7	246	11.1	11.5
	Spring (n=9)	122	1.43	1.28	1.42	371	14.1	20.1	68.9	229	9.41	9.97
	Summer (n=12)	54.6	0.676	0.471	0.354	65.1	9.31	4.57	14.7	65.3	3.20	4.01

652 Autumn: Sep-Nov, 2013; Winter: Dec 2013-Feb 2014; Spring: Mar-May, 2014; Summer: Jun-Aug, 2014.

653 Table 2. The annual and seasonal average concentrations of OC and EC and secondary inorganic ions (NO_3^-, SO_4^{2-}, and NH_4^+) (μg m^{-3}) and ratios
654 of OC/EC and NO_3^-/SO_4^{2-} in Shanghai.

	Annual (n=116)	Autumn (n=26)	Winter (n=36)	Spring (n=31)	Summer (n=23)
OC	9.89 ± 8.89	7.00 ± 8.38	17.2 ± 10.5	7.50 ± 2.62	4.92 ± 3.12
EC	1.63 ± 1.53	0.990 ± 0.840	2.88 ± 2.03	1.30 ± 0.620	0.840 ± 0.460
POC	3.32 ± 3.11	2.03 ± 1.72	5.87 ± 4.14	2.64 ± 1.27	1.71 ± 0.95
SOC	6.56 ± 6.68	4.97 ± 6.89	11.3 ± 8.25	4.86 ± 1.71	3.33 ± 2.37
OC/EC	6.69 ± 2.64	7.36 ± 2.84	6.90 ± 3.14	6.41 ±1.88	5.99 ± 2.03
	Annual (n=69)	Autumn (n=16)	Winter (n=28)	Spring (n=15)	Summer (n=10)
Cl^-	2.64 ± 2.06	1.58 ± 1.50	4.98 ± 3.48	0.930 ± 0.510	0.390 ±0.240
NO_3^-	18.0 ± 19.1	15.0 ± 18.2	29.1 ± 21.2	10.4 ± 5.35	2.80 ±3.61
SO_4^{2-}	14.5 ± 9.61	12.9 ± 9.30	19.5 ± 9.98	12.3 ± 6.53	6.68 ± 3.79
K^+	1.28 ± 1.81	0.940 ± 0.920	1.65 ± 0.810	0.700 ± 0.270	1.70 ± 4.24
NH_4^+	8.13 ± 6.99	6.64 ± 6.22	12.6 ± 7.22	5.48 ± 3.60	2.09 ± 2.06
NO_3^-/SO_4^{2-}	1.05 ± 0.57	0.980 ± 0.650	1.42 ± 0.400	0.890 ± 0.320	0.380 ± 0.250

655

656 Table 3. The mean soluble concentrations (ng m^{-3}, mean ± S.D.) and fractions (%, mean
657 ± S.D.) of trace metals in $PM_{2.5}$ from Shanghai on pollution days and non-pollution days.

	Pollution days (n=12)		Non-pollution days (n=9)	
	Concentration	Fraction	Concentration	Fraction
Cr	2.20 ± 0.800	15.5 ± 7.50	1.07 ± 0.540	10.8 ± 2.55
Cu	8.84 ± 5.69	41.4 ± 12.5	1.83 ± 0.900	27.8 ± 5.05
Pb	14.2 ± 8.06	18.1 ± 4.99	5.58 ± 4.66	19.2 ± 3.67
Zn	60.5 ± 72.1	17.1 ± 11.7	5.16 ± 4.07	4.45 ± 2.72
V	7.18 ± 4.59	69.9 ± 15.7	6.13 ± 3.86	83.7 ± 6.24
Ni	1.78 ± 0.840	22.9 ± 13.6	1.37 ± 0.550	26.3 ± 9.14

658

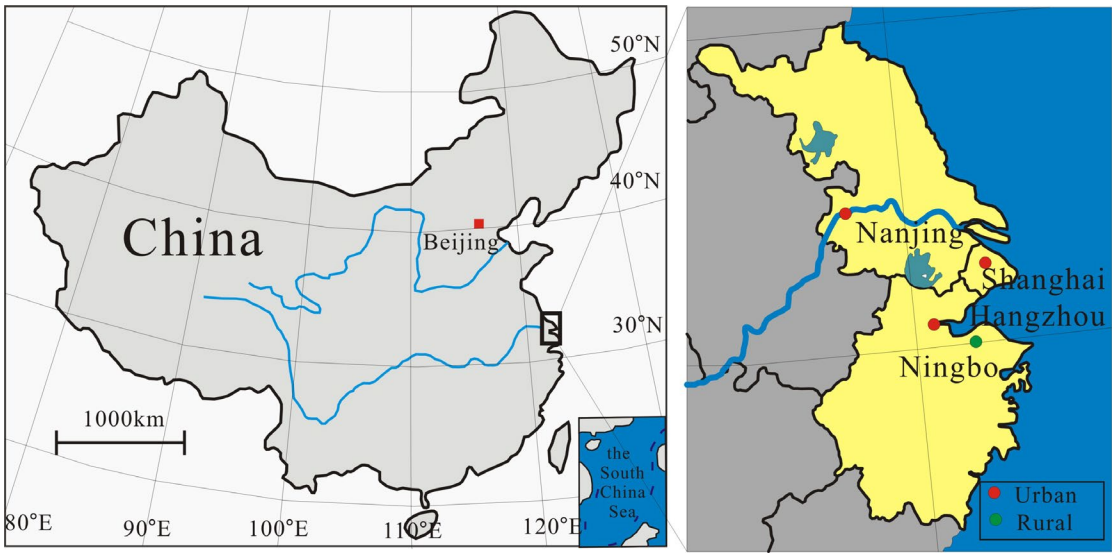

Figure 1. The four sampling sites in the Yangtze River Delta, China.

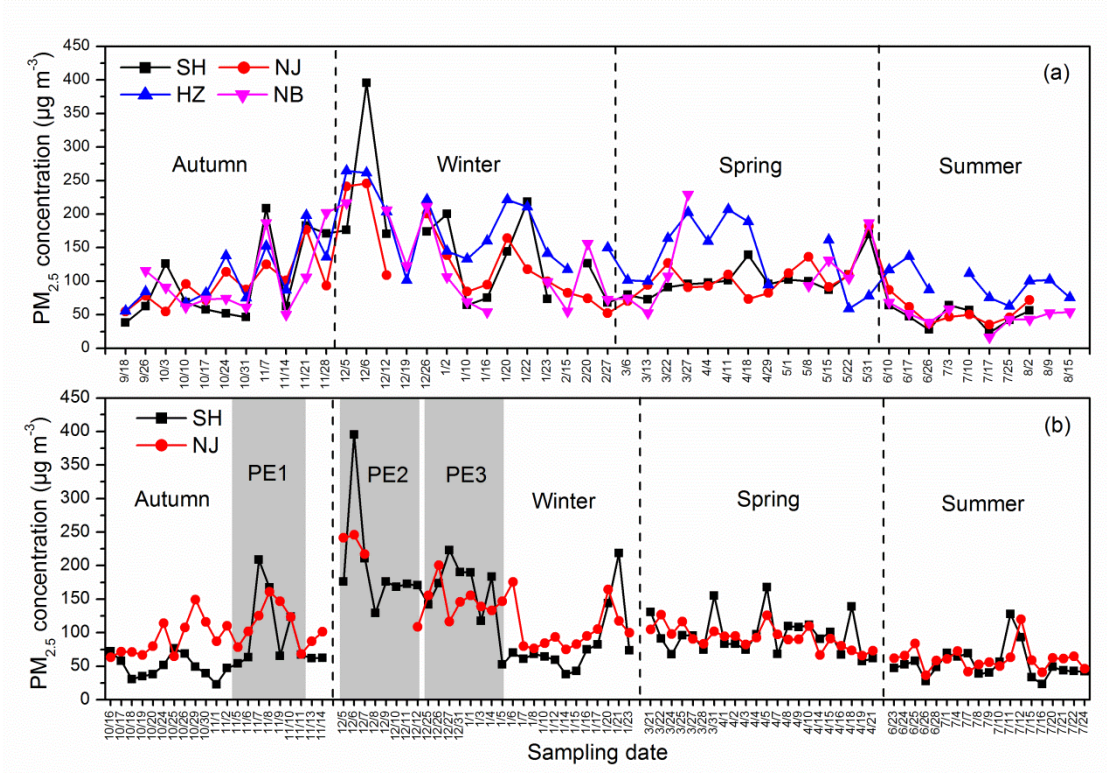

Figure 2. Temporal variations in $PM_{2.5}$ concentrations: (a) for the simultaneous samples from Shanghai, Nanjing, Hangzhou, and Ningbo; and (b) for the samples collected during the high-frequency sampling period in Shanghai and Nanjing.

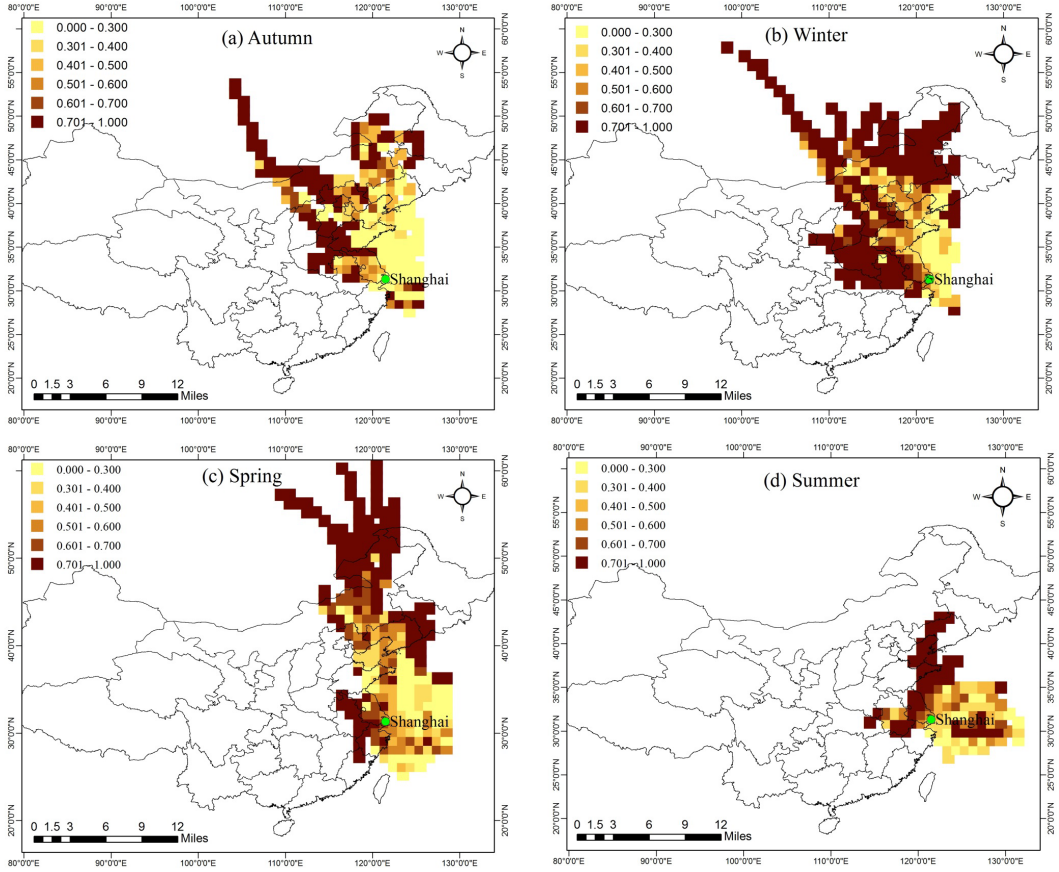

676

677 Figure 3. Maps of potential sources of $PM_{2.5}$ in Shanghai during the four seasons. The

678 darkness of the red cells represents PSCF values.

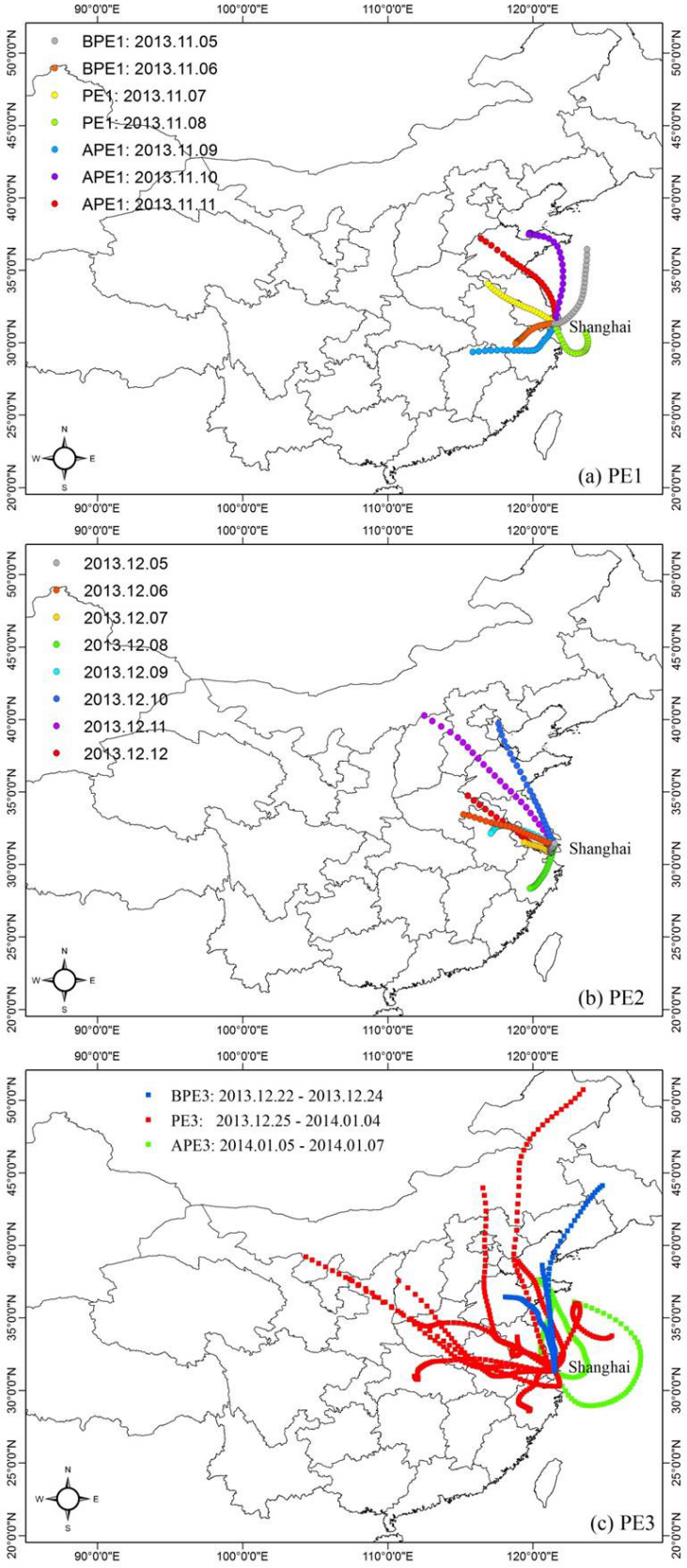

679

680 Figure 4. One-day backward trajectories of air masses arriving in Shanghai at an
681 altitude of 1000 m in the course of the three pollution events: (a) PE1; (b) PE2; and (c)

682 PE3.

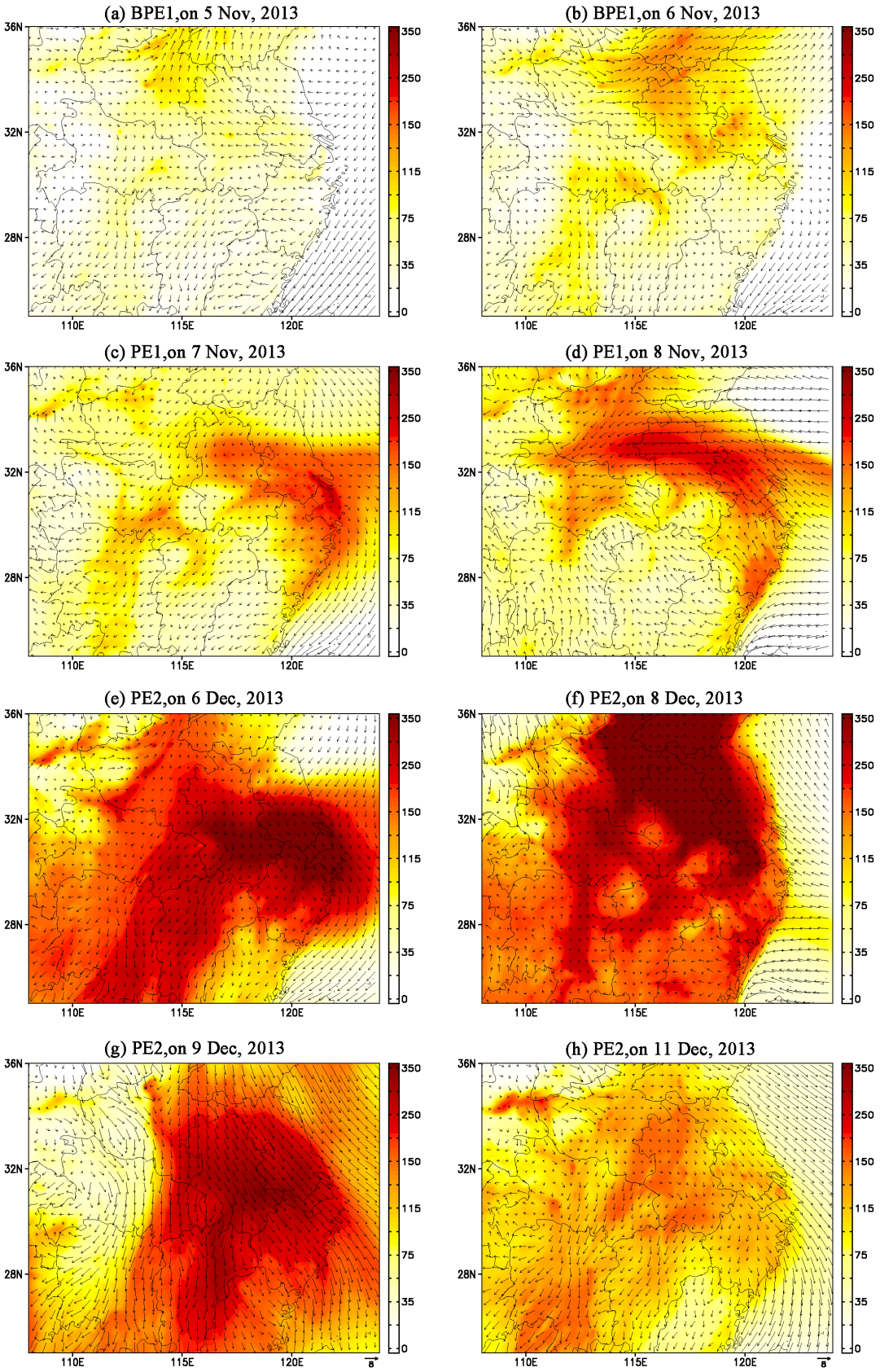
(a) BPE1,on 5 Nov, 2013
(b) BPE1,on 6 Nov, 2013
(c) PE1,on 7 Nov, 2013
(d) PE1,on 8 Nov, 2013
(e) PE2,on 6 Dec, 2013
(f) PE2,on 8 Dec, 2013
(g) PE2,on 9 Dec, 2013
(h) PE2,on 11 Dec, 2013
36N
32N
28N
110E
115E
120E
350
250
150
115
75
35
0

683

Figure 5. The simulated daily average of surface $PM_{2.5}$ concentrations (μg m^{-3}) and wind vectors (m s^{-1}) in eastern China: (a) BPE1, on 5 Nov, 2013; (b) BPE1, on 6 Nov, 2013; (c) PE1, on 7 Nov, 2013; (d) PE1, on 8 Nov, 2013; (e) PE2, on 6 Dec, 2013; (f) PE2, on 8 Dec, 2013; (g) PE2, on 9 Dec, 2013; and (h) PE2, on 11 Dec, 2013.

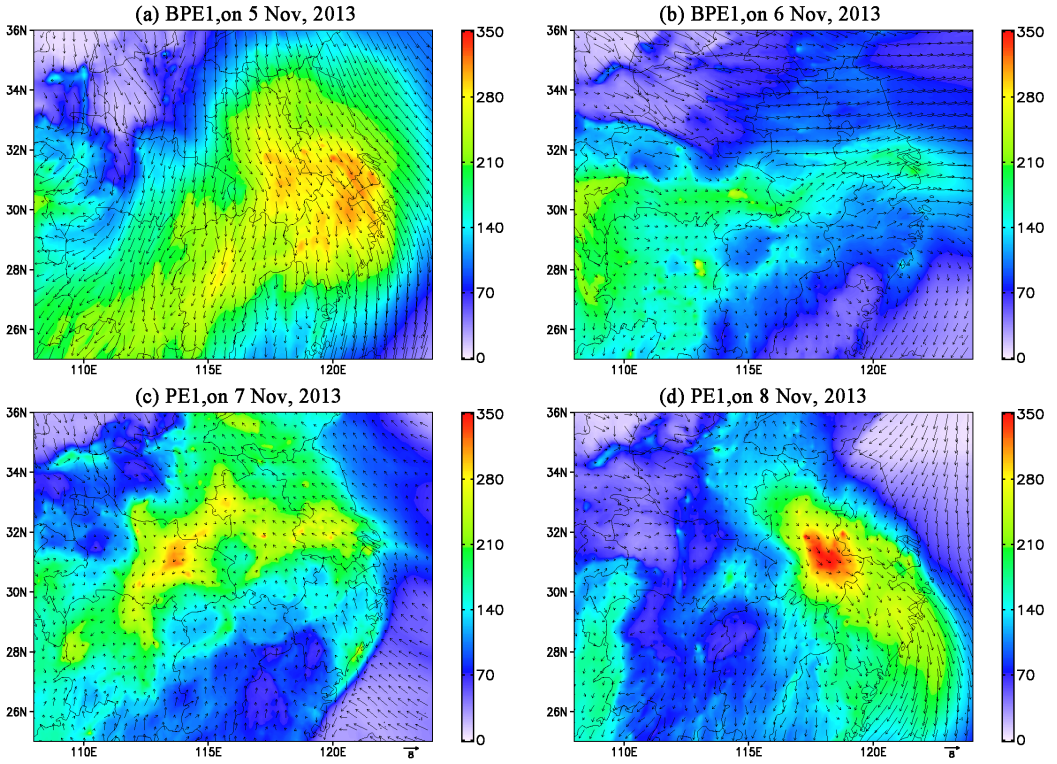

Figure 6. The simulated daily average of surface $PM_{2.5}$ concentrations (μg m^{-3}) and wind vectors (m s^{-1}) in eastern China: (a) PE3, on 26 Dec, 2013; (b) PE3, on 31 Dec, 2013; (c) PE3, on 2 Jan, 2014; and (d) PE3, on 4 Jan, 2014.

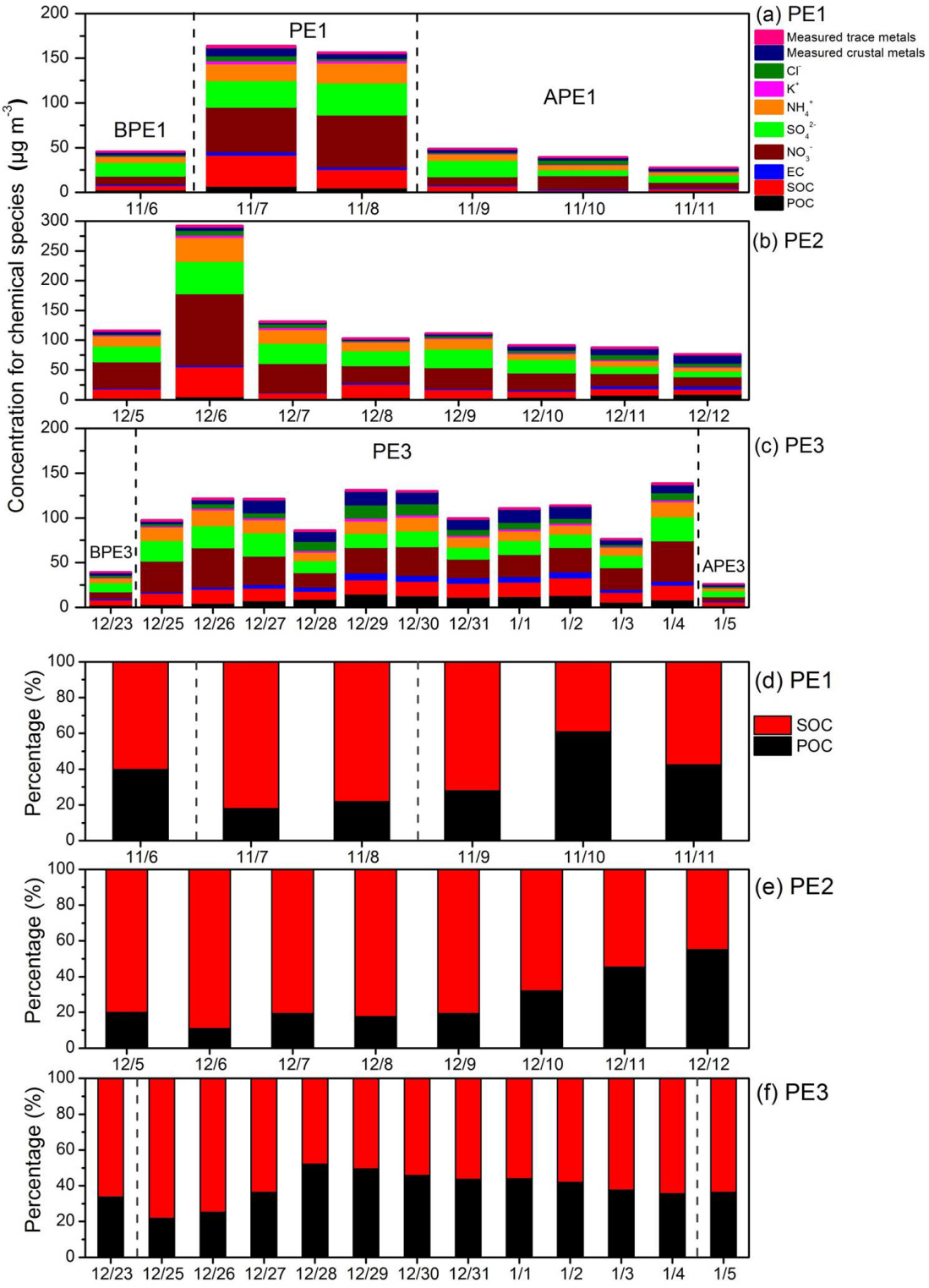

692

693 Figure 7. Concentrations of the measured chemical compositions and the relative
694 abundance of primary organic carbon (POC) and secondary organic carbon (SOC) in
695 the $PM_{2.5}$ samples from Shanghai during the three pollution processes.

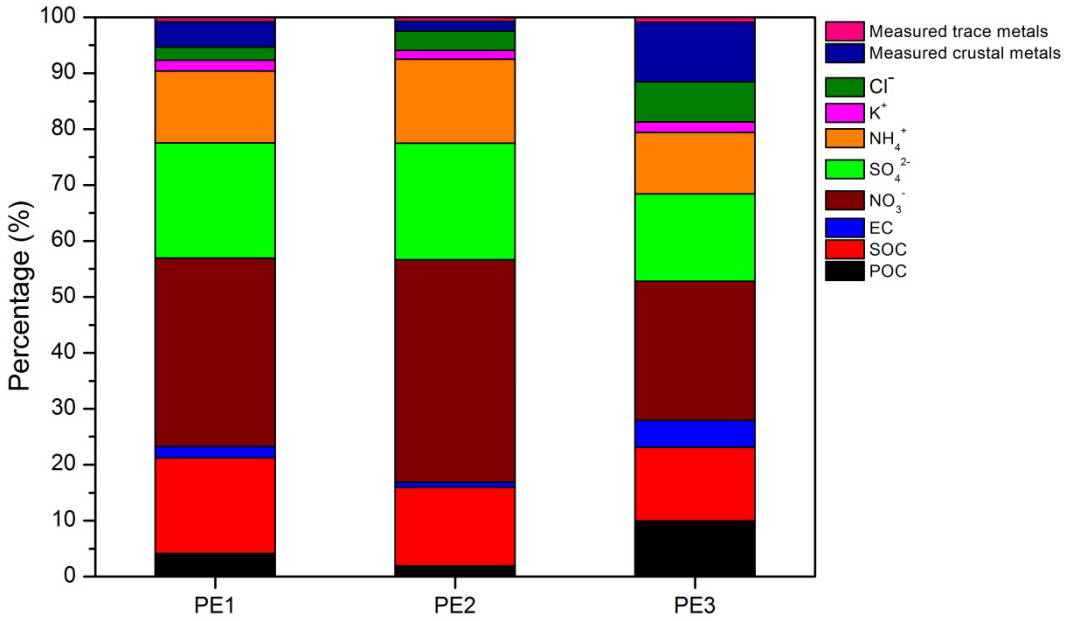

696

697 Figure 8. Relative abundance of the measured chemical compositions in the $PM_{2.5}$
698 samples from Shanghai during the three pollution events: PE1, 7-8 Nov, 2013; PE2, 5-
699 12 Dec, 2013; and PE3, 25 Dec, 2013-5 Jan, 2014.